THE JOURNAL OF BIOLOGICAL CHEMISTRY VOL. 282, NO. 26, pp. 19144–19151, June 29, 2007

Saltatory Forward Movement of a Poly(A) Polymerase during Poly(A) Tail Addition*

Received for publication, January 8, 2007, and in revised form, April 27, 2007 Published, JBC Papers in Press, May 8, 2007, DOI 10.1074/jbc.M700183200

Janice M. Yoshizawa, Changzheng Li, and Paul D. Gershon[1]

From the Department of Molecular Biology and Biochemistry, University of California, Irvine, California 92697

Vaccinia poly(A) polymerase (VP55) interacts with ≥33-nucleotide (nt) primers via uridylates at two sites (−27/−26 and −10). It adds ~30-nt poly(A) tails with a rapid, processive burst in which the first few nt are added without substantial primer movement, and addition of the remaining adenylates is dependent upon a six-uridylate tract at the extreme 3′ end of the primer and accompanied by polymerase translocation. Interaction of VP55 with 2-aminopurine (2-AP)-containing primers was associated with a 3-fold enhancement in 2-AP fluorescence. In stopped-flow experiments, fluorescence intensity changed with time during the polyadenylation burst in a manner dependent upon the position of 2-AP, indicating a non-uniform isomerization of the polymerase-primer complex with time consistent with a discontinuous (saltatory) translocation mechanism. Three distinct translocatory phases could be discerned: a −10(U)-binding site forward movement, a −27/−26(UU)-binding site jump to −10, then a −27/−26(UU)-binding site movement further downstream. Poly(A) tail elongation showed no apparent pauses during these isomerizations. Fluorescence changes during polyadenylation of 2-AP-containing primers with short preformed oligo(A) tails reinforced the above observations. Primers composed entirely of oligo(U) (apart from the 2-AP sensor), in which the polymerase modules might be most able to "slide" uniformly, also showed the characteristic saltatory pattern of translocation. These data indicate, for the first time, a discontinuous mode of translocation for a non-templated polymerase.

Poly(A) polymerase (PAP),[2] the enzyme responsible for adding the poly(A) tail to mRNA and other (1, 2) RNAs, is found in a variety of organisms including eukaryotes, prokaryotes, and viruses (3). PAP acts as a nucleic acid template-independent NMP-transferase, preferentially utilizing a single species of NTP, namely ATP.

Vaccinia virus is a member of the poxvirus family and, like eukaryotes, has post-transcriptionally 5′-capped and 3′-polyadenylated mRNAs (4). In contrast to the monomeric eukaryotic and bacterial PAPs, the vaccinia PAP (VP55) is found as a 1:1 complex with its processivity factor VP39 (5, 6). In the absence of VP39, oligo(A) tails are added to permissive primers by VP55 in a rapid processive burst, which ceases abruptly after tails have reached 30–35 nucleotides in length (7). Permissive primers for the burst are ≥33 nt in length and possess a three-uridylate ($(rU)_2$-N_{15}-rU "VP55-binding") motif positioned ~10 nt upstream from the 3′-OH (8, 9). However, primers possessing no uridylates other than the VP55-binding motif (9) receive no more than ~3–7 adenylates in the burst. With an additional UNUUUUU ("translocatory") motif positioned at the extreme 3′ end of the initial primer, the full 30–35 adenylate tail can be added (10). When VP55 is allowed to synthesize its own binding site by conversion to a poly(U) polymerase in the presence of Mn^{2+}, tails hundreds of nucleotides in length are processively synthesized with no abrupt cessation of elongation (11), demonstrating translocation of the polymerase to the newly synthesized tail.

PAP crystal structures have shed light on non-templated polymerase catalytic mechanism and architecture. The structures of two eukaryotic (bovine and yeast) PAPs have been reported (12, 13), each showing three domains (N-terminal, central, and C-terminal) with the catalytic center in the N-terminal one. This arrangement seems similar to that observed in template-dependent enzymes, except that in the latter, the catalytic center is located in the central domain (12–14). Although bovine and yeast PAPs are structurally very similar to one another, their interaction with substrate analogs appears to be distinct (13, 15). More recently, the crystal structure for the vaccinia VP55-VP39 heterodimer was solved (16), providing insight into the catalytic mechanism, the mode of ATP binding, and the architecture of a PAP-processivity factor complex. The vaccinia PAP showed no structural homology to eukaryotic PAPs outside the immediate vicinity of the catalytic center, and although a three-domain architecture could be perceived, the catalytic center was in the central, not the N-terminal, domain (16).

To our knowledge, other than VP55, none of the reported non-templated nucleic acid polymerases, including eukaryotic and other PAPs, are known to fully translocate with respect to their primers. For example, terminal deoxynucleotidyltransferase (the only reported template-independent DNA polymerase) does not translocate but adopts a strictly non-processive mode of nucleotide addition (17). Eukaryotic PAPs appear to remain tethered via the protein complex CstF/CPSF and/or other components of the mRNA cleavage/polyadenylation complex at the AAUAAA polyadenylation initiation signal during full-length poly(A) tail addition (18–20), with the "reeled-

* This work was supported by National Institutes of Health Grants 5R01GM51953 and 5T32AI007319-19. The costs of publication of this article were defrayed in part by the payment of page charges. This article must therefore be hereby marked "*advertisement*" in accordance with 18 U.S.C. Section 1734 solely to indicate this fact.

[1] To whom correspondence should be addressed: Dept. of Molecular Biology and Biochemistry, Rm. 1222, Natural Sciences I, University of California, Irvine, Irvine, CA 92697. Tel.: 949-824-9606; Fax: 949-824-8551; E-mail: pgershon@uci.edu.

[2] The abbreviations used are: PAP, poly(A) polymerase; VP55, vaccinia PAP; 2-AP, 2-aminopurine; nt, nucleotide; SFFS, stopped-flow fluorescence spectrometry; RQF, rapid quench flow.

out" nascent tail becoming coated by the protein PAB II as it is synthesized (21). The situation regarding RNA uridylyltransferases is unclear (22). Here, we identify steps in the movement of vaccinia VP55 across its primer and onto the nascent tail during tail addition.

EXPERIMENTAL PROCEDURES

Materials—VP55 and VP55-ΔN10 were purified as described (16). Purified proteins had estimated specific activities for polyadenylation of >90%. Oligonucleotides were synthesized via solid phase chemistries using reagents from Glen Research Corp. and Chemgenes Corp. Prior to use, oligonucleotides were purified by urea-PAGE using standard methods.

Steady-state Fluorescence Spectrophotometry and SFFS—80-μl samples of VP55 and oligonucleotide (4 and 2 μM, respectively) in TD buffer (50 mM Tris-HCl, pH 9.0, 2 mM dithiothreitol) were equilibrated at room temperature for 15–30 min. Steady-state fluorescence spectra were then collected at room temperature, using a Hitachi model F-4500 fluorescence spectrophotometer with a sample path length, photomultiplier tube voltage, and scan speed of 3 mm, 700 V, and 240 nm/min, respectively. Excitation spectra were collected at a fixed emission wavelength of 370 nm, and emission spectra were collected at a fixed excitation wavelength of 320 nm, with excitation and emission bandwidths of 5 and 10 nm, respectively. Excitation and emission scan ranges were 250–350 and 330–550 nm, respectively. Bar plots are derived from the fluorescence signal at the 365–370 nm maximum of the scanned peak. In Figs. 5 and 7, $(OP - O)/O = (\text{fluorescence}^{(\text{oligo + Protein})} - \text{fluorescence}^{(\text{oligo only})})/\text{fluorescence}^{(\text{oligo only})}$. Data were processed and overlaid using KaleidaGraph v4.0.

Stopped-flow fluorescence spectrometry (SFFS) measurements employed a Model SX.18MV stopped-flow spectrometer (Applied Photophysics, Leatherhead, UK) with excitation wavelength and slit width of 320 and 1 mm, respectively. Emission intensity was measured via a 335-nm cut-off high-pass filter in combination with an IF435 broad-pass interference filter (Applied Photophysics, 90% transmittance). "Target PMT" (instrument sensitivity) was set to 50 or 70% (for an expected rise or fall, respectively, in fluorescence at the end of the reaction). Prior to firing, syringe 1 was filled with TD buffer containing oligonucleotide (2 μM) and VP55 (3.6–4 μM). Syringe 2 was filled with TD buffer containing ATP (1 mM) and $MgCl_2$ (1 mM). NaCl concentration after mixing (dependent upon NaCl concentration in VP55 protein preparations) was 60–120 mM. After equilibration to room temperature, 0.1 ml was fired simultaneously from syringes 1 and 2 through the mixer. After stopping, fluorescence emission was measured over 10^3 data points. Traces shown in Figs. 3, 5, 7, and 8 are the mean of 2–5 replicate runs with a constant subtracted to normalize the fluorescence intensity (ordinate) value at the outset of the reaction to zero. Data were processed using Microsoft Excel and then plotted and overlaid using KaleidaGraph v4.0.

Rapid Quench Flow (RQF) and Manual Quench Polyadenylation Time Course Assays—The two reagent mixtures were as described for SFFS experiments (above). After equilibration to room temperature, reactions were initiated, either manually by manual rapid mixing or by firing 15-μl aliquots of the respective reagent mixtures simultaneously from syringes 1 and 2 of a four-syringe microvolume quench-flow instrument (QFM-400, BioLogic SA, Grenoble, France, fitted with a 3-μl delay line). Reactions were quenched with 50 mM EDTA (pH 8.0) in formamide either manually or with a 30-μl shot from syringe 4 of the QFM-400 with products collected into 1.5 ml-microtubes. 4-μl aliquots of quenched reactions were resolved in 15% polyacrylamide, 7 M urea gels in standard Tris borate/EDTA buffer. cy3 fluorescence was acquired from wet gels in the cy3 channel of a Molecular Imager FX Pro Plus (Bio-Rad; 532 nm excitation).

RESULTS

The 33-nt oligonucleotide primers used throughout this study contained the VP55-binding motif (8), VP55's translocatory motif (10) and, in most instances, a 5′-cy3 moiety. In all primers, 2-aminopurine deoxyribonucleotide (2-AP, a fluorescent nucleotide) was present at a single non-essential position.

VP55-dependent Enhancement of Oligonucleotide (2-AP) Fluorescence—Our standard downstream 2-AP primer (possessing 2-AP adjacent to the −10(U) of the VP55-binding motif, Fig. 1*A*) showed a broad fluorescence excitation peak attributable to rU, dC (23), and 2-AP (Fig. 1*B*). Upon the addition of excess VP55 to the primer followed by rescanning, excitation spectra showed an ~3-fold increase in fluorescence intensity in the 310–320-nm region (Fig. 1*B*). Fluorescence emission spectra for the primer showed an emission peak centered at 365 nm, which was enhanced 2.9-fold upon the addition of VP55 and rescanning (Fig. 1*C*).

Discontinuous VP55 Translocation—Our standard upstream 2-AP primer (possessing 2-AP at position −25, Fig. 2*A*) exhibited fluorescence excitation and emission spectra almost identical to those of Fig. 1, *B* and *C* (data not shown). The magnitude of VP55-induced fluorescence emission enhancement for the standard upstream and downstream 2-AP primers was virtually identical (~2.9–3-fold; Fig. 2*B*).

The observation of enhanced fluorescence afforded an opportunity to assay isomerization of the VP55-primer complex in real time during poly(A) tail addition, via SFFS. Each of the two standard primers exhibited a distinctive SFFS fluorescence intensity *versus* time profile during the initial 10 s of poly(A) tail addition (Fig. 2*C*), indicating that VP55 interacts asynchronously with regions of the primer immediately adjacent to −27/−26(UU) and −10(U) portions of the VP55-binding motif. The initial notable event on the time trajectory (starting at ~0.25 s, in Fig. 2*C*, labeled *a*) was a loss of fluorescence enhancement for the downstream 2-AP primer, indicating loss of a downstream primer-VP55 contact. The subsequent notable event (first noticeable at ~1.0 s, in Fig. 2*C*, labeled b_1) was a loss of fluorescence enhancement with the upstream 2-AP primer consistent with loss of the upstream contact. This was accompanied by a transient re-emergence of fluorescence enhancement for the downstream 2-AP primer (b_2), consistent with a rebinding of VP55's −27/−26(UU)-binding site in the −10(U) region. Finally (starting at ~1.5 s, in Fig. 2*C*, labeled *c*), there was a loss of this transient fluorescence enhancement, consistent with a movement of VP55's −27/−26(UU)-binding site from the 2-AP at position −9 to a position further down-

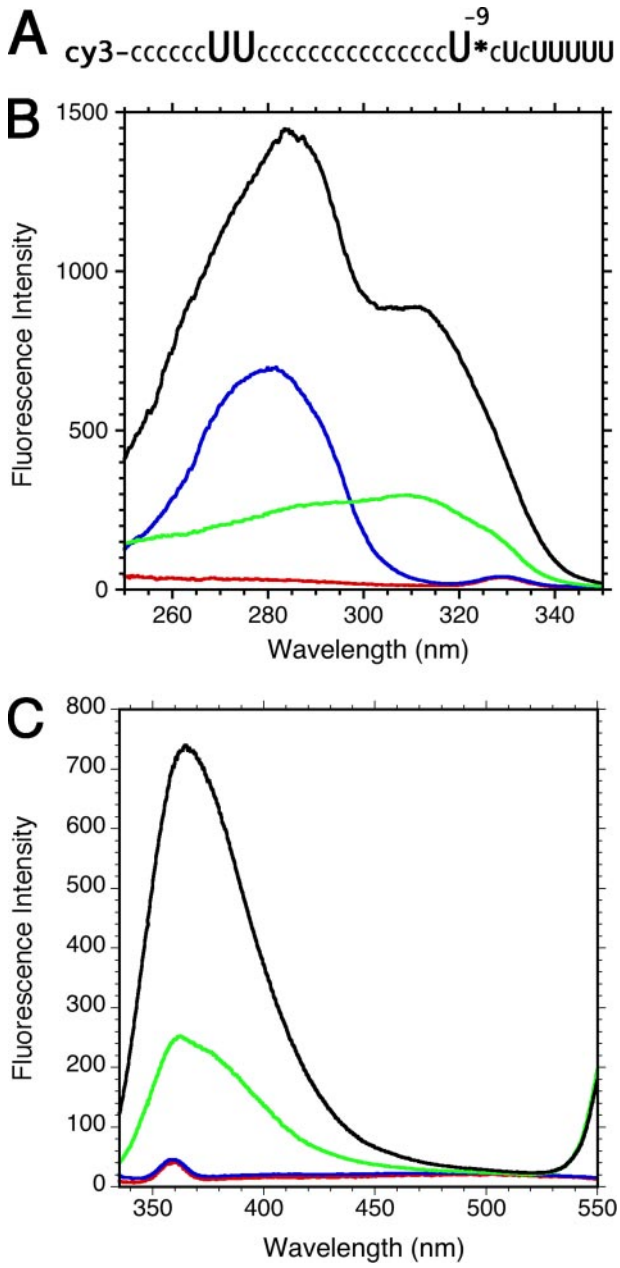

FIGURE 1. **VP55-dependent enhancement in fluorescence of the standard downstream 2-AP primer.** *A*, sequence of standard downstream 2-AP primer. *C*, deoxyC; *U*, riboU (*larger font U*, VP55-binding motif; *smaller font U*, translocatory motif). *, 2-aminopurine deoxyribonucleotide (position −9). *B* and *C*, fluorescence excitation and emission spectra, respectively, for standard downstream 2-AP primer. Ordinates are in arbitrary units. *Red*, *blue*, *green*, and *black traces*, buffer, VP55, primer, VP55+primer, respectively.

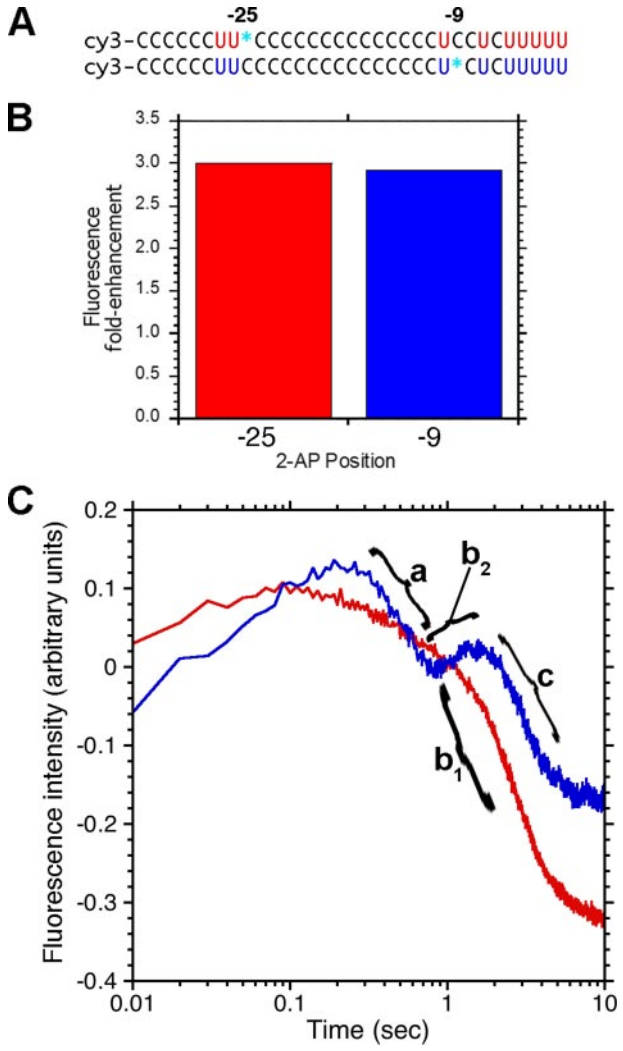

FIGURE 2. **Fluorescence emission changes upon elongation of 2-AP-containing model primers.** *A*, sequences of standard upstream (*upper*) and downstream (*lower*) 2-AP primers (*lower*, identical to Fig. 1, see the legend for Fig. 1 (*panel A*)). Sequences are colored as a reference for *panels B* and *C* and for Fig. 3. *B*, -fold enhancement in steady-state fluorescence emission after equilibrating primers with excess VP55. Oligonucleotides lacking 2-AP entirely showed no detectable fluorescence emission under the conditions employed (data not shown). K_d of 4×10^{-7} M for VP55-primer interaction, estimated from fluorescence concentration measurements (data not shown), was consistent with previous measurements (10) and severalfold below the primer/protein concentrations employed here. *C*, SFF profiles. Each profile represents the mean of 2–3 replicate experiments. *a*–*c*, time-dependent features (phases) as described under "Results."

stream. The absence of synchronized isomerization at the two 2-AP sites (Fig. 2) was consistent with molecular flexibility in either the polymerase or the primer or both during the initial stages of translocation by VP55, and therefore, saltatory translocation.

To establish whether the fluorescence changes observed by SFFS were truly dependent upon primer elongation, control oligonucleotides were synthesized identical to the two standard primers, except for replacement of the 3′-most riboU with dideoxyT. Since the 3′-OH ordinarily serves as the initial attacking nucleophile in the polymerization reaction, the absence of this moiety prevented polymerization but did not affect primer-polymerase affinity determinants. SFFS experiments (Fig. 3, *A* and *B*, performed under conditions identical to those of Fig. 2*C*) showed no significant fluorescence changes for the control primers, indicating that the fluorescence changes of Fig. 2*C* were dependent upon actual primer elongation as opposed to, for example, Mg·ATP-protein interaction.

Continuous Tail Elongation Accompanies Polymerase-Primer Isomerizations—Poly(A) tail lengths were assayed at specific points in the SFFS time line (Fig. 4). Time points prior to the first SFFS isomerization in Fig. 2*C* (50–200 ms) showed tails mostly 5 nt or shorter, the range of tail lengths that can be synthesized with the polymerase bound to just the VP55-binding motif (9). 1–12-nt-tailed products accumulated during the

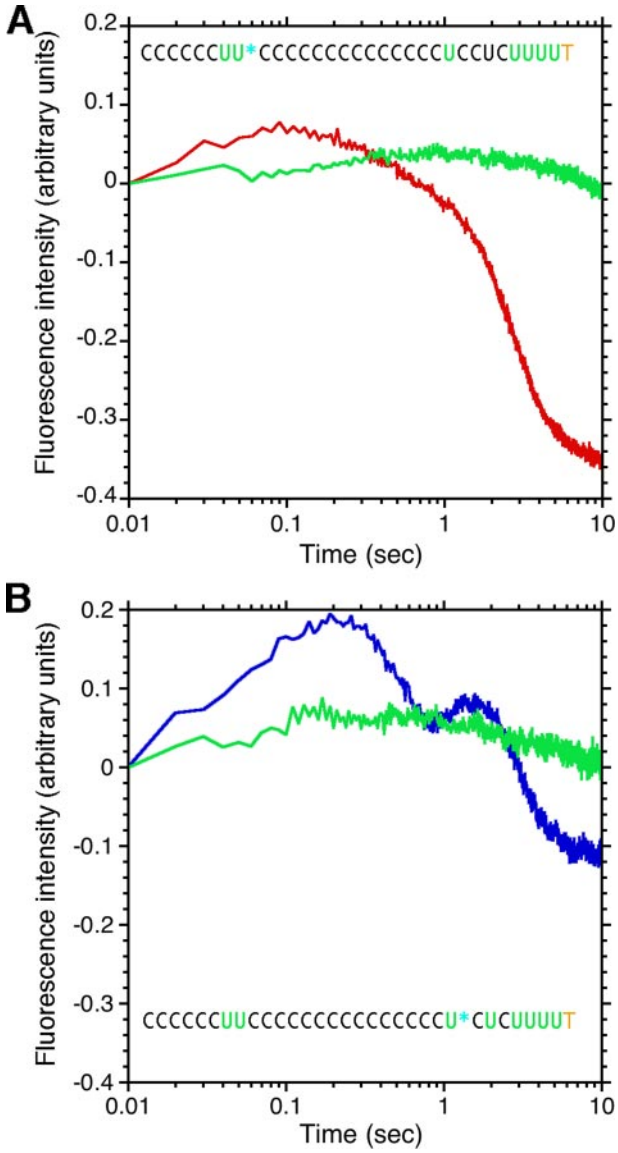

FIGURE 3. *A* and *B*, SFFS profiles for upstream 2-AP and downstream 2-AP dideoxyoligonucleotides, respectively. Dideoxy oligonucleotides (*green uridylates* and *traces*) were identical to the standard primers (Fig. 2) except for replacement of the 3-terminal U with dideoxyT (lacking 2′-OH and 3′-OH; shown in *orange*). Traces for standard primers are copied from Fig. 2*C* for comparison. Each profile represents the mean of 2–3 replicate experiments.

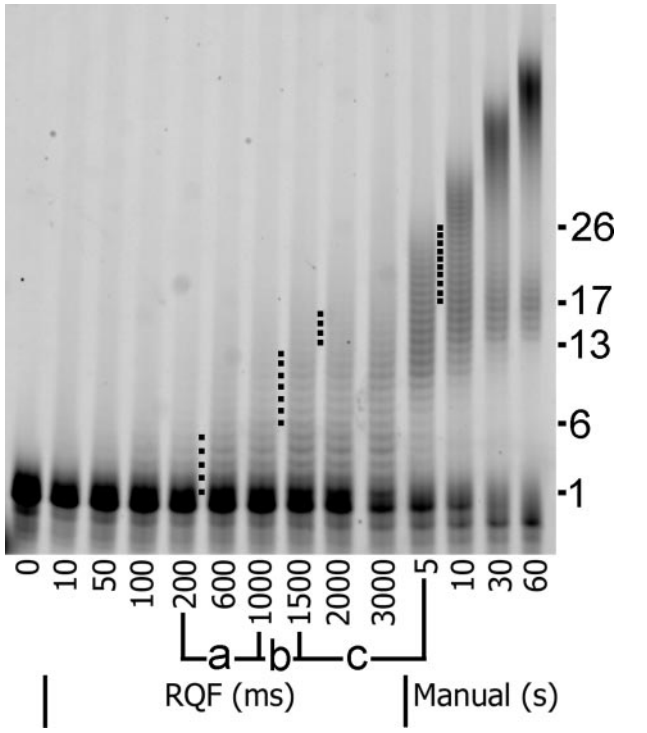

FIGURE 4. **Continuous tail elongation accompanies polymerase-primer isomerizations.** A standard upstream 2-AP primer (sequence, Fig. 2*A*) was subjected to RQF (10–3000 ms) and manual quench (5–60 s) polyadenylation time course assays under SFFS experimental conditions other than quenching after specified reaction times. *a–c*, phases in Fig. 2*C*. *Right*, tail lengths (in nt) corresponding to dotted single adenylate increments. Lighter exposure showed abundance of initial primer, dropping rapidly at the outset of the RQF assay to ~33% the level of usable starting primer, depleting the remainder after the 3-s time point (data not shown). The initial processive cycle of tail addition thus followed rapid saturation of ~67% of the primer with polymerase. The zero time point was take prior to assays.

200–1000-ms interval (Fig. 4), corresponding to SFFS phase a (Fig. 2*C*). Between 1000 and 1500 ms (corresponding to Fig. 2*C*, phase b_1/b_2,), 1–16-nt products appeared. Between 1.5 and 5 s (corresponding to Fig. 2*C*, *phase c*), 7–26-nt products (full-length tails) began to appear. The processive round was considered complete by ~5 s in the assay of Fig. 4, consistent with both VP55's known inability to processively elongate tails beyond ~26–35 nt and the cessation of the phase c fluorescence drop in Fig. 2*C*. However, *in vitro*, some elongation typically continues in a much slower, non-processive mode (7) as visible in the 5–60-s time points of Fig. 4 (this non-processive mode was relatively rapid under the conditions of polymerase excess employed here). The resistance of some 17–20 adenylate-tailed products to non-processive elongation (Fig. 4) may have been due to primer "masking" under the conditions of polymerase excess. In conclusion, the polymerase catalytic center appears to progress more or less uniformly notwithstanding isomerization of polymerase-primer contacts further upstream.

2-AP Adjacent to the Translocatory Motif Detects Additional, Distinct Polymerase Contacts—To determine whether alternative sites of 2-AP within the primer could detect distinct profiles, three additional primers were synthesized containing 2-AP at positions −20, −15, or −6 (Fig. 5*A*). Steady-state fluorescence emission measurements in the absence and presence of VP55 (Fig. 5*B*) indicated a diminished fluorescence enhancement for the 2-AP positions not adjacent to essential uridylates (−20, −15). This did not arise from a lowered affinity (data not shown) and was therefore attributed to diminished fluorescence coupling.

SFFS polyadenylation profiles are shown in Fig. 5*C*. With respect to the profile for the standard downstream 2-AP primer, repositioning of 2-AP six nucleotides further upstream (to position −15) did not lead to a new fluorescence profile, but instead, to a less pronounced version of that for the standard downstream 2-AP primer. The absence of a new profile indicated that contact at position −15 is not within an independently mobile domain of VP55 but is within the same one that interacts at −9/−10. The less pronounced signal (consistent with the weaker fluorescence enhancement in Fig. 5*B*) indicated that either polymerase contact with 2-AP at −15 is less

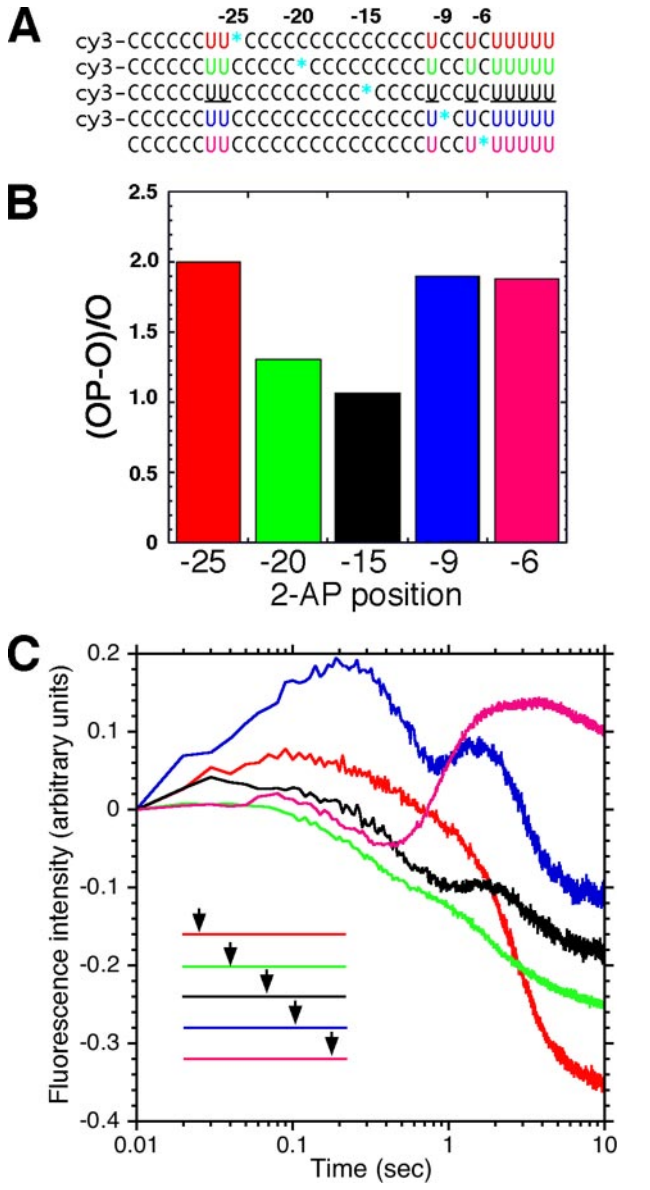

FIGURE 5. **2-AP adjacent to the translocatory motif detects a polymerase contact late during the polyadenylation cycle.** *A*, primer sequences. Uridylates are color-coded as a reference for *panels B* and *C* (primers with *red*, *blue uridylates* as shown in Fig. 2*A*). *B*, enhancement in steady-state fluorescence emission due to VP55. On the ordinate, *0* represents no fluorescence enhancement; *1* represents doubling of oligonucleotide fluorescence intensity; *2* represents tripling, etc. *Red* and *blue bars*, data of Fig. 2*B* plotted as (OP − O)/O. *C*, SFFS profiles. Each profile represents the mean of 3–4 replicate experiments. *Arrow*, 2-AP position within the primer. Traces for standard primers are copied from Fig. 2*C* for comparison.

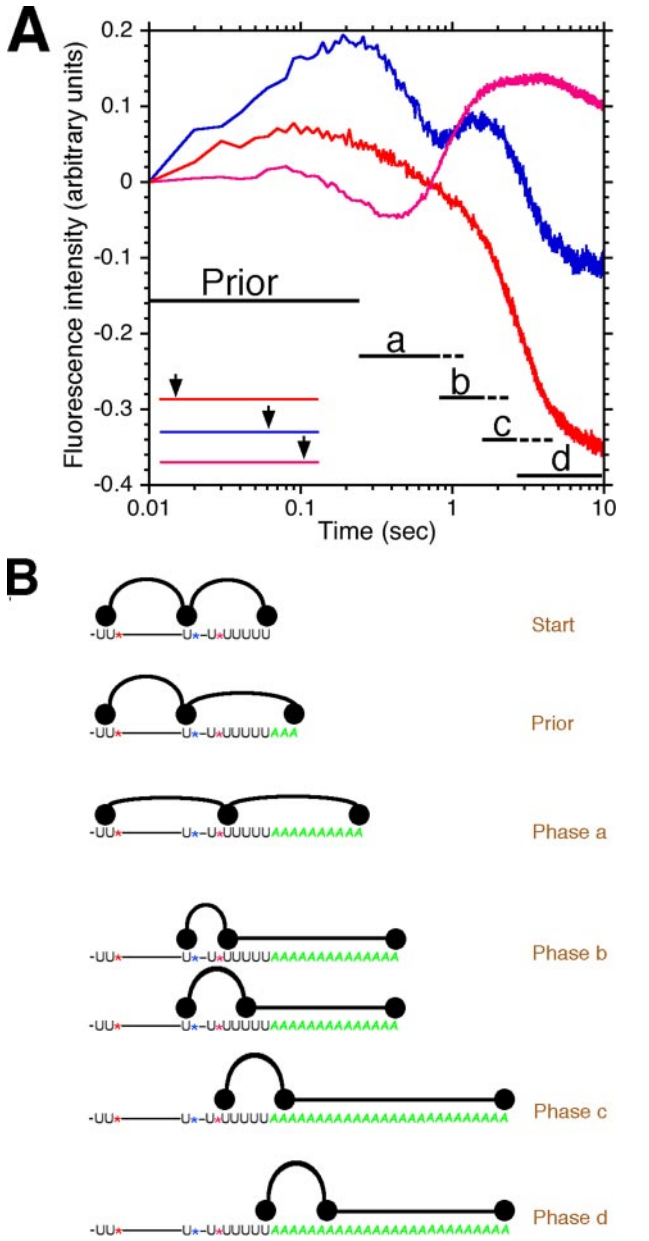

FIGURE 6. **Model of translocation.** *A*, the three distinct fluorescence profiles identified here (from Figs. 2*C* and 5*C*) reproduced on the same plot for direct comparison of three 2-AP positions and elucidation of the four phases of elongation indicated on the time line. *B*, primer contacts by three regions of VP55 polymerase (*black filled circles*) during the phases of translocation indicated in *panel A*. *Rightmost region*, catalytic center. Other regions represent U-recognition sites.

prone to fluorescence enhancement or 2-AP located at −15 detected only a minor population with respect to a thermodynamically more favorable one in which VP55's fluorescence-enhancing site contacts position −9. Repositioning 2-AP an additional 5 nt further upstream (to position −20) also did not lead to a new profile, but instead, to an apparent hybrid of the standard downstream and upstream profiles (2-AP at position −9 and −25, respectively). Thus, the −20 position either overlaps the upstream-binding and downstream-binding domains of VP55 or is distributed between complexes in which it is bound to either one. Again, the less pronounced trace was consistent with the less pronounced fluorescence enhancement in Fig. 5*B*. The final primer, in which 2-AP was positioned closer to the 3′ end (position −6), showed a novel profile with an early, sustained, rise in fluorescence enhancement.

The three distinct fluorescence profiles observed thus far (Figs. 2 and 5) are interpreted in terms of VP55 translocatory steps (Fig. 6). During the first ~0.25 s (prior), the first few adenylates are added to the tail prior to any isomerization of uridulate-VP55 contacts. During phase a, VP55's downstream uridylate-binding site dissociates from −10(U) (loss of enhancement, *blue trace*) and rebinds around −7U (gain in enhancement, *pink trace*). During phase b, VP55's upstream

uridylate-binding site dissociates from −27/−26(UU) (loss of enhancement, *red trace*) and rebinds −10(U) gain in enhancement, *blue trace*). In Fig. 6*B*, this is quickly followed by a downstream movement in the downstream U-binding site to restore spacing between VP55's two U-binding sites. Although the *pink trace* (Fig. 6*A*) appears to show a broad peak in fluorescence enhancement, this is interpreted as two overlapping peaks (elongation becoming less synchronous later in the tail addition cycle), the first of which is dropping at the end of phase b, consistent with the restoration of spacing mentioned above. During phase c, VP55's upstream uridylate-binding site dissociates from −10(U) (second loss of enhancement, *blue trace*) and binds −7(U) (*pink trace*, second broad peak). Phase d represents the disengagement of VP55 from all three uridylate sensors. During the above process, it is proposed that the catalytic center tracks the 3′ end monotonically, consistent with the apparently uniform (pause-free) tail elongation apparent in Fig. 4. Although Fig. 6*B* shows VP55 only undergoing isomerization as translocation progresses, this is for ease of depiction and does not rule out changes in the topology of the primer.

Defined Intermediates of Processive Tail Elongation—Primers with short preformed oligo(A) tails (mimicking polyadenylation intermediates, Fig. 7*A*) were synthesized containing 2-AP adjacent to the downstream U of the VP55-binding motif (a position at which SFFS data showed the greatest information content, Fig. 2*C*). Steady-state fluorescence emission measurements indicated a magnitude of fluorescence enhancement that was inversely related to the length of preformed tail (Fig. 7*B*). This was consistent with a fluorescence-enhancing region of VP55 falling in register with the RNA 3′-OH, leading to its progressive movement away from the 2-AP sensor with increasing tail length.

SFFS experiments (Fig. 7*C*) reinforced and extended these conclusions. When compared with the downstream 2-AP primer lacking a preformed tail (Fig. 6*A*; in which phases a, b2, and c initiated at ~0.2, 0.8, and 1.5 s, respectively), the primer with a preformed AA tail initiated the three phases earlier in the time line (at ~0.02, 0.5 and 1.0 s, respectively). With preformed tails of 4, 6 or 8 adenylates, phase a (the initial drop in fluorescence) was no longer detected (Fig. 7*C*; consistent with the lower fluorescence enhancement upon initial binding Fig. 7*B*). This was presumably because, with the longer preformed tail, the downstream domain had already moved away from its starting position over 2-AP. Consistent with the 4-, 6-, and 8-nt tail primers representing intermediates in VP55's processive polyadenylation cycle, phase b_2 (the rebinding event) occurred progressively earlier with increasing preformed tail length (initiating at 0.3, 0.2, and 0.1 s, respectively). We conclude that primers possessing preformed oligo(A) tails mimic *bona fide* translocation intermediates and that VP55's downstream U-binding site advances progressively during the early stages of tail elongation.

Discontinuous Translocation Is Obligatory—The primers used for the experiments of Figs. 2–7 possessed no uridylates other than those essential for VP55 binding and synthesis of a full-length, 25–30-nt poly(A) tail (see the Introduction). Other sequence positions were filled with dC. To address the possibility that we may have forced a discontinuous mode of translocation upon VP55 by use of primers with significant non-ribouridylate tracts, primers were synthesized with 2-AP at positions equivalent to those of Fig. 2 but embedded within uniform oligo(U) tracts (Fig. 8*A*). In SFFS experiments (Fig. 8*B*), time-dependent fluorescence changes were not coordinated between the upstream and downstream 2-AP positions, indicating that, even when given an opportunity to "slide" monotonically over an isoenergetic oligo(U) tract, VP55's preferred mode of translocation was discontinuous with regard to the most major isomerization events. Fluorescence profiles in Fig. 8*B* differed in subtler ways from those of the standard primers (Fig. 2*C*); for example, phase a started immediately upon initiating polyadenylation (without a 0.2-s pause), phase b was more prolonged (0.3–3 s), and phase c started later (3 s) and was not complete by the end of the assay (10 s). To better understand these differences, tail length data were acquired for one of the oligo(U)-

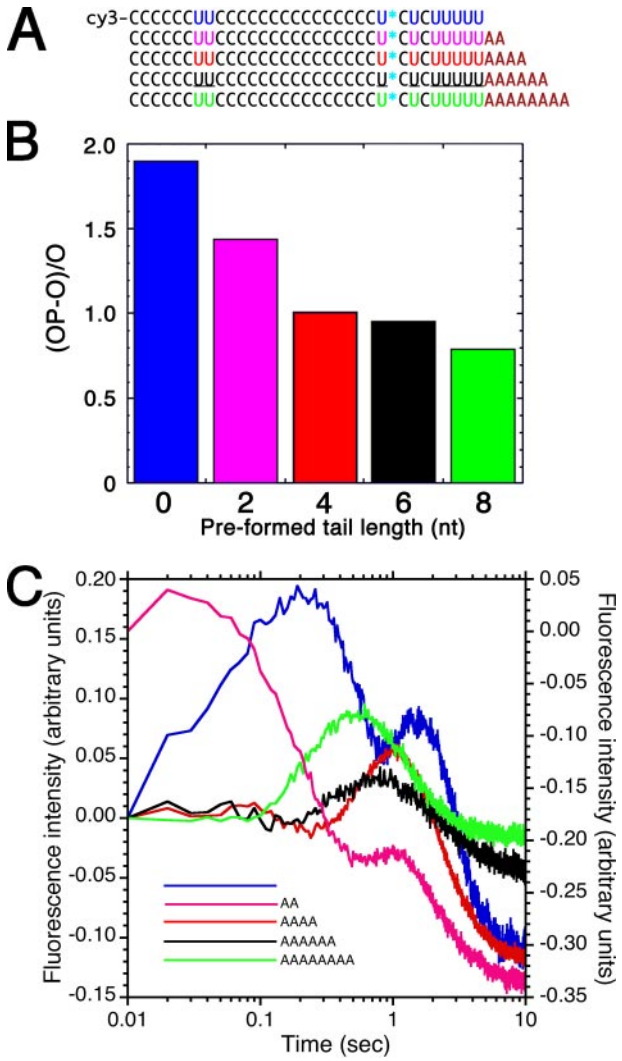

FIGURE 7. **Defined intermediates of processive tail elongation, represented by primers with short preformed oligo(A) tails.** *A*, primer sequences based on the standard primer with 2-AP at position −9 (*lower sequence*, Fig. 2*A*). * = riboA. *B*, enhancement in steady-state fluorescence emission due to VP55, with other details as in Fig. 5*B*. In separate experiments, polymerase-primer K_d was indistinguishable for the 8- and 0-nt tail primers (data not shown), eliminating this as a cause for the observed fluorescence differences. *C*, SFFS profiles. Each profile represents the mean of 3–5 replicate experiments. *Left scale*, all primers except that with 2-nt tail (*mauve*). *Right scale*, 2-nt tail primer (offset, since fluorescence started high). Data for the primer with no preformed tail were reproduced from Fig. 2*C*.

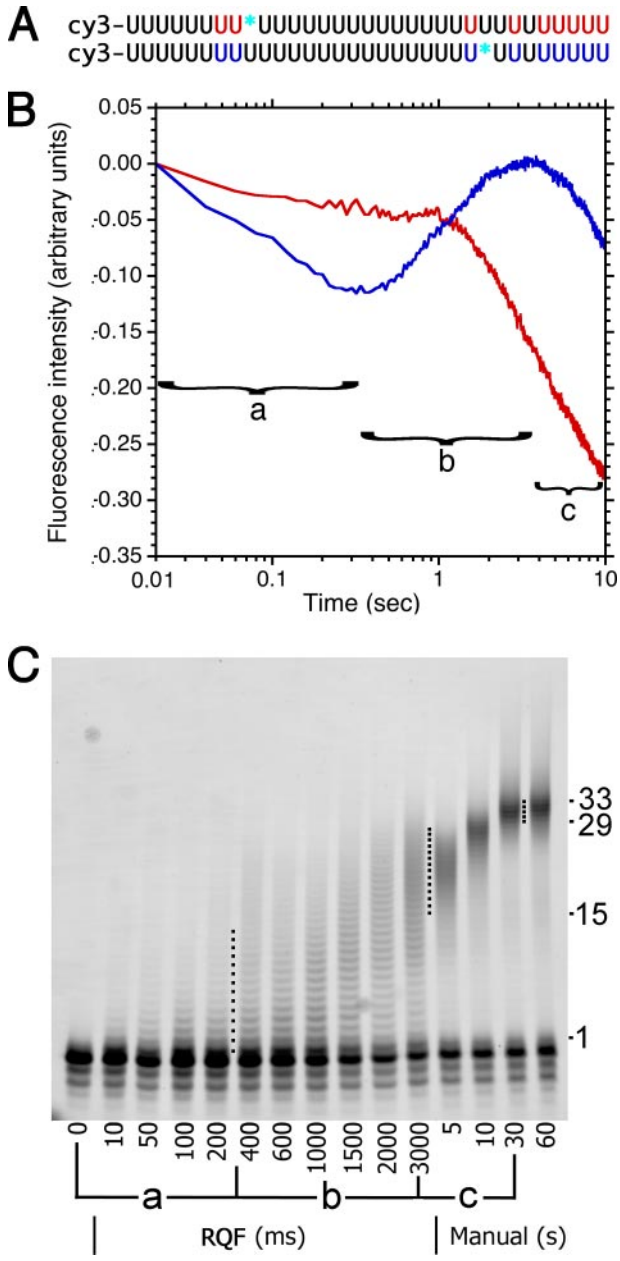

FIGURE 8. **Primers composed of oligo(rU) tracts.** *A*, primer sequences, colored as a reference for *panel B* (details in the legend for Fig. 1 (*panel A*); 2-AP positions equivalent to model primers in Fig. 2*A*). *B*, SFFS profiles. Each profile represents the mean of 3 replicate experiments. *Phases a*, *b*, and *c* correspond to phases *bracketed* in Fig. 2*C*. *C*, polyadenylation time course assay of upper primer from *panel A*, with other details as for Fig. 4.

based primers (Fig. 8*C*). Tails were first visible at 10 ms (as opposed to 100 ms with the standard downstream primer, Fig. 4), with the oligo(U) primer receiving up to 14 adenylates by 100 ms. Apparently, the presence of the uniform oligo(U) tract between position −10 and the 3′-OH eliminated any initial pause in the forward movement of the downstream U-binding domain. In phase b, tails were elongated to 28 nt. Tails continued to be elongated processively between ~3 and 30 s (Fig. 8*C*), consistent with the markedly slower and more prolonged phase c (Fig. 8*B*). There may be a greater number of rebinding options for VP55's −27/−26(UU)-binding site during phase c with oligo(U) primers, with some complexes imperfectly orientated for rapid completion of processive tail addition or for exposure of the 3′-OH for the subsequent non-processive phase.

DISCUSSION

Here, translocation of the vaccinia poly(A) polymerase, VP55, was monitored as a function of time during processive addition of the complete ~25–30-nt poly(A) tail via continuous, real-time changes in 2-AP fluorescence enhancement arising from isomerization of the VP55-primer complex. Since VP55 does not interact with 2-AP in a way that promotes protein-RNA interaction (VP55 recognizes uridylates only, and all essential uridylates were already present within primers), 2-AP apparently acts independently of RNA recognition. However, it provided the strongest and most unique signals only when adjacent to essential uridylates of the primer. Fluorescence enhancement may have arisen from a localized destacking of weakly or partially stacked bases within the single-stranded oligonucleotide upon polymerase binding, perhaps due to engagement of the polymerase with the uridylate adjacent to the 2-AP. Alternatively, there may be some form of direct electronic coupling of the 2-AP nucleobase with aromatic side chains of VP55 present in the vicinity of the uridylate recognition sites.

The primers used in the first part of this study were RNA·DNA chimeras. The use of such chimeras with VP55 is entirely consistent with prior studies. Thus, although RNA primers were shown long ago to be inactive when resynthesized as all-DNA, when the DNA's dT residues were substituted with rU, full primer activity was restored (11). This finding has subsequently been sustained, exploited, and extended (8–10, 24–26). The current study exploits the above finding without inconsistency or conflict.

Albeit that the SFFS experiments were monitoring the major population of primer molecules at any one time, the lack of abruptness in fluorescence changes was consistent with the distribution of tail lengths observed in RQF experiments at each time point (Fig. 4). Use of a much stronger quench in quench-flow experiments (alkaline SDS, data not shown) did not narrow the product distribution, arguing against non-instantaneous quenching. Due to the processivity of VP55, premature termination by the polymerase during the assay was also presumably not responsible for asynchrony. However, asynchrony could have arisen from non-uniform initiation times or elongation rates.

The data presented here and interpreted in Fig. 6 extend a prior study that provided static "snapshots" of VP55's primer contacts during the addition of the first ~10 adenylates of the tail, via partial hydrolysis of primer molecules possessing preformed oligo(A) tails and essential uridylate positions as mixed rU/dC pools after substrate selection by VP55 (10). As in the current study, a three-module polymerase was required to account for the data. Isomerizations during phases a and b of the current study are in complete agreement with the prior study. Although the prior study was able to correlate changes in contact more precisely with changes in tail length, contacts could not be monitored clearly for primers with tails >~10 nt in length. The current experiments provide a more complete picture of changes in polymerase-primer contact, continuously, and in real time during poly(A) tail elongation. Moreover, the

experiments in Fig. 7 of the current study showed that primers with preformed tails mimic *bona fide* translocation intermediates, validating the selection approach taken previously (10). The two complementary approaches are strikingly consistent, and the model of Fig. 6 provides an overall picture, demonstrating later steps that could only be speculated in the prior study (10).

Overall, the data demonstrate a saltatory translocation mechanism for VP55, the first such demonstration for a non-templated nucleic acid polymerase.

Acknowledgments—We thank Sufeng Zhou for help in expression and purification of VP55, Dr. Tom Poulos for use of the fluorescence spectrophotometer and stopped-flow spectrometer and members of the Poulos laboratory for assistance, Dr. Steen Pedersen (Baylor College of Medicine) for the use of a stopped-flow spectrometer and help with preliminary experiments.

REFERENCES

1. Kadaba, S., Wang, X., and Anderson, J. T. (2006) *RNA* (*Cold Spring Harbor*) **12,** 508–521
2. LaCava, J., Houseley, J., Saveanu, C., Petfalski, E., Thompson, E., Jacquier, A., and Tollervey, D. (2005) *Cell* **121,** 713–724
3. Manley, J. L. (1995) *Proc. Natl. Acad. Sci. U. S. A.* **92,** 1800–1801
4. Moss, B. (2001) in *Fields Virology* (Fields, B. N., ed) 4th Ed., pp. 2849–2883, Lippincott, Williams & Wilkins, Philadelphia
5. Moss, B., Rosenblum, E. N., and Gershowitz, A. (1975) *J. Biol. Chem.* **250,** 4722–4729
6. Gershon, P. D., Ahn, B.-Y., Garfield, M., and Moss, B. (1991) *Cell* **66,** 1269–1278
7. Gershon, P. D., and Moss, B. (1992) *Genes Dev.* **6,** 1575–1586
8. Deng, L., and Gershon, P. D. (1997) *EMBO J.* **16,** 1103–1113
9. Deng, L., Beigelman, L., Matulic-Adamic, J., Karpeisky, A., and Gershon, P. D. (1997) *J. Biol. Chem.* **272,** 31542–31552
10. Johnson, L., Liu, S., and Gershon, P. D. (2004) *J. Mol. Biol.* **337,** 843–885
11. Gershon, P. D., and Moss, B. (1993) *EMBO J.* **12,** 4705–4714
12. Bard, J., Zhelkovsky, A. M., Helmling, S., Earnest, T. N., Moore, C. L., and Bohm, A. (2000) *Science* **289,** 1346–1349
13. Gershon, P. D. (2000) *Nat. Struct. Biol.* **7,** 819–821
14. Martin, G., Keller, W., and Doublie, S. (2000) *EMBO J.* **19,** 4193–4203
15. Hall, T. M. (2002) *Curr. Opin. Struct. Biol.* **12,** 82–88
16. Moure, C. M., Bowman, B. R., Gershon, P. D., and Quiocho, F. A. (2006) *Mol. Cell* **33,** 339–349
17. Delarue, M., Boule, J. B., Lescar, J., Expert-Bezancon, N., Jourdan, N., Sukumar, N., Rougeon, F., and Papanicolaou, C. (2002) *EMBO J.* **21,** 427–439
18. Bienroth, S., Keller, W., and Wahle, E. (1993) *EMBO J.* **12,** 585–594
19. Zhao, J., Hyman, L., and Moore, C. (1999) *Microbiol. Mol. Biol. Rev.* **63,** 405–445
20. Calvo, O., and Manley, J. L. (2001) *Mol. Cell* **7,** 1013–1023
21. Kuhn, U., and Wahle, E. (2004) *Biochim. Biophys. Acta* **1678,** 67–84
22. Aphasizhev, R. (2005) *CMLS Cell. Mol. Life Sci.* **62,** 2194–2203
23. Cavaluzzi, M. J., and Borer, P. N. (2004) *Nucleic Acids Res.* **32,** e13
24. Gershon, P. D. (1998) *Semin. Virol.* **8,** 343–350
25. Deng, L., Johnson, L., Neveu, J. M., Hardin, S., Wang, S.-M., Lane, W. S., and Gershon, P. D. (1999) *J. Mol. Biol.* **285,** 1417–1427
26. Oguro, A., Johnson, L., and Gershon, P. D. (2002) *Chem. Biol.* **9,** 679–690